Check for updates

Received: 3 August 2020 | Revised: 14 November 2020 | Accepted: 10 January 2021

DOI: 10.1002/aic.17202

SEPARATIONS: MATERIALS, DEVICES AND PROCESSES

AIChE JOURNAL

Enhanced weathering to capture atmospheric carbon dioxide: Modeling of a trickle-bed reactor

Lei Xing | Richard C. Darton | Aidong Yang

Department of Engineering Science, University of Oxford, Oxford, UK

Correspondence
Aidong Yang, Department of Engineering Science, University of Oxford, Oxford OX1 3PJ, UK.
Email: aidong.yang@eng.ox.ac.uk

Funding information
Natural Environment Research Council, Grant/Award Number: NE/P01982X/1

Abstract

Enhanced weathering (EW) of alkaline minerals can potentially capture CO_2 from the atmosphere at gigaton scale, but the reactor design presents great challenges. We model EW with fresh water in a counter-current trickle flow packed bed batch of 1–10 mm calcite particles. Weathering kinetics are integrated with the mass transfer of CO_2 incorporating transfer enhancement by chemical reaction. To avoid flooding, flow rates must be reduced as the particles shrink due to EW. The capture rate is mainly limited by slow transfer of CO_2 from gas to liquid although slow dissolution of calcite can also play a role in certain circumstances. A bed height of at least 7–8 m is required to provide sufficient residence time. The results highlight the need to improve capture rate and reduce energy and water consumption, possibly through enriching the feed with CO_2 and further chemical acceleration of the mass transfer.

KEYWORDS
carbon dioxide removal, enhanced weathering, enhancement factor, mathematic modeling, trickle bed reactor

1 | INTRODUCTION

Although the rate at which greenhouse gases are accumulating in the atmosphere could be reduced by cutting emissions, elevated levels of CO_2 will remain for centuries.[1] Climate models show that peak CO_2-induced global warming is mainly determined by cumulative CO_2 emissions, rather than the emission pathway.[2] As a consequence, it may well become necessary to remove large amounts of CO_2 from the atmosphere—a process known as carbon dioxide removal (CDR). The IPCC has warned that "All pathways that limit global warming to 1.5°C with limited or no overshoot project the use of CDR on the order of 100–1000 $GtCO_2$ over the 21st century."[3,4]

Among the potential routes to CDR, enhanced weathering (EW) based on the exposure of crushed alkaline minerals to the atmosphere is a promising option. In chemical terms, EW is similar to the process of liming fields to reduce their acidity, as practiced by farmers for centuries.[5] Currently, the weathering of rock by carbon dioxide and water, a natural process, absorbs about 1.1 Gt CO_2 per year from the atmosphere, mainly stored as bicarbonate in the ocean.[6] Many types of carbonate and silicate mineral show CO_2 sequestration ability.[7-11] An advantage of the EW approach to CDR is that the CO_2 is captured in the form of carbonate or bicarbonate ions, removing the need for CO_2 compression and underground storage. A potential disadvantage is that, in cases where the bicarbonate ion is a product, chemistry occurring in the natural environment can reverse the reaction, releasing CO_2 again to the atmosphere. A further challenge is the potential scale of operations and the need to handle many tons of crushed rock, and also very large amounts of water, for every ton of CO_2 sequestered. Moreover, it is known that rates of natural weathering are relatively low, and it is not certain that these can be enhanced to an extent sufficient to make EW useful in countering climate change in this century. For the implementation of EW, suggestions include spreading crushed minerals on the soil[8,9] or in coastal environments,[10] and heap leaching.[11] Exploring the potential of a more "engineered"

This is an open access article under the terms of the Creative Commons Attribution License, which permits use, distribution and reproduction in any medium, provided the original work is properly cited.
© 2021 The Authors. *AIChE Journal* published by Wiley Periodicals LLC. on behalf of American Institute of Chemical Engineers.

approach, the motivation for the modeling study presented here is to quantify capture rates and water and energy requirements for an EW process taking place in a chemical reactor. We chose calcite as a model mineral, because its weathering kinetics have been relatively well-studied. By modeling the behavior of a known chemical system in equipment with well-known characteristics we provide a benchmark for process requirements and illustrate the technical issues that might arise when attempting EW at a large scale, in a novel setting.

The dissolution of calcite in the CO_2-water system was first ascribed to three simultaneous reactions occurring at the solid–liquid interface by Plummer et al.[12] They also drew attention to the importance of pH. Buhmann and Dreybrodt[13] developed a model for the water film sandwiched between a plane calcite surface and atmosphere. They found that reaction at the calcite surface was the rate-limiting process when the fluid was in turbulent flow, but in laminar flow the rate-limiting process strongly depended on the ratio of the volume of the solution and the surface area of calcite. Their later work[14] confirmed that the conversion of CO_2 into HCO_3^- was the rate-limiting process when the liquid film on the calcite surface was very thin. The studies of rate-limiting processes provided valuable insights to the mechanisms of weathering of calcite. However, most previous work was limited to batch reactors operated with a CO_2 pre-saturated solution.[12-14] The mass transport of CO_2 from atmosphere into liquid was rarely integrated with the kinetics of calcite weathering.

The reactor type studied in this work is the packed bed column, which is very widely used in the process industries for carrying out both reactions and separations in multi-phase systems. In this work, we consider the use of packed bed columns for EW, where the reacting mineral particles are contacted with air and water and provide interfacial area for gas–liquid mass transfer. An important feature of the process is that the calcite particles change size during dissolution, which alters the bed hydrodynamics as the reaction proceeds. We also consider the possible advantages of using air enriched with carbon dioxide, and the benefits of increasing the rates of reaction (e.g., by catalysis) to accelerate the mass transfer. The resulting model provides useful guidance on the design and operation of a trickle flow packed bed for CO_2 sequestration through EW.

2 | MODEL DEVELOPMENT

2.1 | Main assumptions

In the mathematical model we integrate the transport of CO_2 from gas to liquid with the kinetics of calcite dissolution and liquid-phase reactions in a trickle flow packed bed which is illustrated in Figure 1. The following are the main assumptions used:

- Solid particles are loaded into the reactor at the start of the operation, with no further replenishment.
- The flow arrangement in the reactor is counter-current. Water enters at the top, air at the bottom.
- A one-dimensional model is developed to describe the spatial variation of concentrations through the height of the cylindrical packed bed. No radial gradients of concentration or velocity are considered.
- The velocities of gas and liquid are assumed not to vary along the bed height.
- An average particle-shrinking rate is applied to all calcite particles, independent of the location inside the packed bed. The particles retain their shape (assumed spherical) during dissolution.
- The ability of the chemical reactions to accelerate the rate of carbon dioxide absorption is taken into account by the use of enhancement factors.

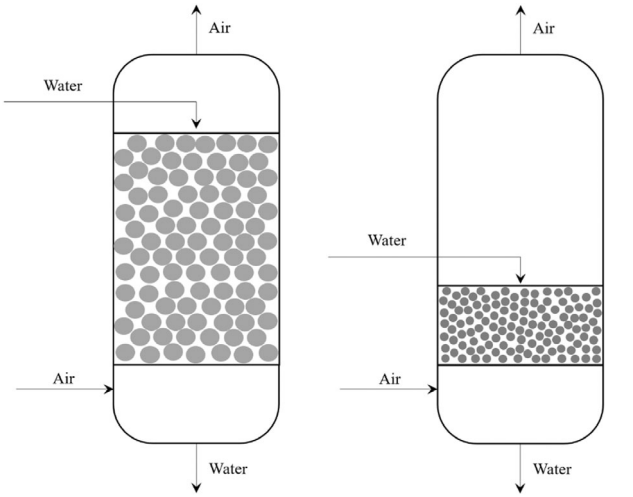

FIGURE 1 Schematic of the trickle flow packed bed reactor: left—at the beginning, right—during enhanced weathering (EW) reaction

2.2 | Mass conservation and boundary conditions

For CO_2 in the gas phase, diffusive and dispersive mass transport is negligible compared to convection (Peclet number $\gg 1$) and is therefore omitted from consideration. An unsteady state mass balance for $CO_{2(g)}$ over a volume element of the bed yields for the gas phase

$$\varepsilon_G \frac{\partial}{\partial t} c_{CO_2(g)} + u_G \nabla \cdot c_{CO_2(g)} = -r_{G-L} \quad (1)$$

where ε_G is gas holdup, defined as the volume fraction of the bed occupied by gas phase and r_{G-L} (mol m^{-3} s^{-1}) is the source term, representing transfer of CO_2 from gas to liquid. u_G (m s^{-1}) is the gas superficial velocity.

An unsteady state mass balance for aqueous species i over a volume element of the bed is given by:

$$\varepsilon_L \frac{\partial}{\partial t} c_i - \varepsilon_L D_{i,L} \nabla^2 c_i + u_L \nabla \cdot c_i = r_i \quad (2)$$

where ε_L is liquid holdup, defined as the volume fraction of the bed occupied by liquid phase, u_L (m s^{-1}) is the superficial liquid velocity, c_i

(mol m^{-3}) is the concentration of species *i* in the liquid phase, $D_{i,L}$ (m^2 s^{-1}) is the hydrodynamic dispersion coefficient of species *i* in liquid, and r_i (mol m^{-3} s^{-1}) is the source term of species *i*. The aqueous species include $CO_{2(aq)}$ and Ca^{2+}, and we define the total carbon ions (TCI), to be the sum of HCO_3^- and CO_3^{2-}:

$$c_{TCI} = c_{HCO_3^-} + c_{CO_3^{2-}} \tag{3}$$

The boundary condition of Equation (1) is:

$$\text{at gas inlet, } x = 0, c_{CO_{2(g)}} = c_{CO_{2(g)},\text{inlet}} \tag{4}$$

The boundary conditions of Equation (2) are the Danckwerts' boundary conditions[15]:

$$\text{at liquid inlet}: x = H_{bed},\ u_L c_{i,inlet} = u_L c_i - D_{L,i}\ \nabla c_i,$$

$$\text{at liquid outlet}: x = 0, \nabla c_i \tag{5}$$

The subscript *i* represents the aqueous species, for example, $CO_{2(aq)}$, Ca^{2+} and TCI.

2.3 | Reaction kinetics

The reactions involved in weathering of calcite are as follows[16,17]

$$CO_{2(aq)} + OH^- \underset{k_{12}}{\overset{k_{11}}{\rightleftarrows}} HCO_3^- \tag{6}$$

$$HCO_3^- + OH^- \underset{k_{22}}{\overset{k_{21}}{\rightleftarrows}} CO_3^{2-} + H_2O \tag{7}$$

$$H^+ + OH^- \underset{k_{32}}{\overset{k_{31}}{\rightleftarrows}} H_2O \tag{8}$$

$$CO_{2(aq)} + H_2O \underset{k_{42}}{\overset{k_{41}}{\rightleftarrows}} HCO_3^- + H^+ \tag{9}$$

$$CaCO_{3(s)} + H^+ \underset{k_{52}}{\overset{k_{51}}{\rightleftarrows}} Ca^{2+} + HCO_3^- \tag{10}$$

$$CaCO_{3(s)} + CO_{2(aq)} + H_2O \underset{k_{62}}{\overset{k_{61}}{\rightleftarrows}} Ca^{2+} + 2HCO_3^- \tag{11}$$

$$CaCO_{3(s)} + H_2O \underset{k_{72}}{\overset{k_{71}}{\rightleftarrows}} Ca^{2+} + HCO_3^- + OH^- \tag{12}$$

The rates of reaction and equilibria in the aqueous phase are modeled, with steps (7) and (8) assumed to be in equilibrium, as follows:

$$r_{CO_2(aq)} = r_{G\text{-}L} + \varepsilon_L\left(k_{12}c_{HCO_3^-} - k_{11}c_{CO_2(aq)}c_{OH^-} + k_{42}c_{HCO_3^-}c_{H^+} - k_{41}c_{CO_2(aq)}\right) + a_w\left(k_{62}c_{Ca_2^{2+}}c_{HCO_3^-}^2 - k_{61}c_{CO_2(aq)}\right) \tag{13}$$

$$c_{CO_3^{2-}} = K_2 c_{HCO_3^-} c_{OH^-} \tag{14}$$

$$K_3 c_{H^+} c_{OH^-} = 1 \tag{15}$$

$$r_{Ca^{2+}} = a_w[k_{51}c_{H^+} - k_{52}c_{Ca^{2+}}c_{HCO_3^-} + k_{61}c_{CO_2(aq)} - k_{62}c_{Ca^{2+}}c_{HCO_3^-}^2 + k_{71} - k_{72}c_{Ca^{2+}}c_{HCO_3^-}c_{OH^-}] \tag{16}$$

where a_w (m^{-1}) is the wetted area of solids per unit volume of the bed.

The source term of TCI is:

$$r_{TCI} = \varepsilon_L\left(k_{12}c_{HCO_3^-} - k_{11}c_{CO_2(aq)}c_{OH^-} + k_{42}c_{HCO_3^-}c_{H^+} - k_{41}c_{CO_2(aq)}\right) + a_w\left[k_{51}c_{H^+} - k_{52}c_{Ca^{2+}}c_{HCO_3^-} + 2\left(k_{62}c_{Ca_2^{2+}}c_{HCO_3^-}^2 - k_{61}c_{CO_2(aq)}\right) + k_{71} - k_{72}c_{Ca^{2+}}c_{HCO_3^-}c_{OH^-}\right] \tag{17}$$

The values and sources of rate and equilibrium constants are listed in Table 1.

The composition of the inlet liquid is calculated assuming saturation with CO_2 at atmospheric conditions, by solving the following algebraic equations:

$$c_{CO_2(aq),\text{inlet}} - p_{CO_2,\text{atmos}}/k_H = 0 \tag{18}$$

$$c_{HCO_3^-,\text{inlet}} - K_4 c_{CO_2(aq),\text{inlet}}/c_{H^+,\text{inlet}} = 0 \tag{19}$$

$$c_{CO_3^{2-},\text{inlet}} - K_2 c_{HCO_3^-,\text{inlet}} c_{OH^-,\text{inlet}} = 0 \tag{20}$$

$$c_{H^+,\text{inlet}} c_{OH^-,\text{inlet}} - K_W = 0 \tag{21}$$

$$c_{OH^-,\text{inlet}} + c_{HCO_3^-,\text{inlet}} + 2c_{CO_3^{2-},\text{inlet}} - c_{H^+,\text{inlet}} = 0 \tag{22}$$

where $p_{CO_2,atmos}$ (Pa) is the partial pressure of CO_2 in the atmosphere and k_H (Pa m^3 mol^{-1}) is Henry's constant for CO_2 in water, which can be expressed, with ρ_L in kg m^{-3}, as a function of temperature[19]:

$$k_H = \frac{1}{\rho_L}\exp(-6789.04/T - 11.4519\log T - 0.010454T + 94.4914) \tag{23}$$

The values of parameters defining the base-case condition are given in Table 2.

2.4 | Mass transfer, interfacial areas and phase fractions

In Equation (1), r_{G-L} (mol m^3 s^{-1}) is the source term for the mass transfer of CO_2 from atmosphere into the aqueous phase, which may be expressed as:

$$r_{G-L} = a_{G-L}K_{OL}\left(c^*_{CO_2(aq)} - c_{CO_2(aq)}\right) \tag{24}$$

TABLE 1 Rate constants and equilibrium constants

Parameter	Value	Unit	Reference
K_1	K_4/K_W	$m^3\ mol^{-1}$	Calculated
K_2	$10^{(1568.9/T-2.5866-6.737\times10^{-3}T)}$	$m^3\ mol^{-1}$	16, 18
K_3	$1/K_W$	$m^6\ mol^{-2}$	Calculated
K_4	$\rho_W \exp^{(-12092.1/T\ -\ 36.7816\ln T\ +\ 235.482)}$	$mol\ m^{-3}$	19
K_5	$K_C/(K_2\ K_W)$	$mol\ m^{-3}$	Calculated
K_6	$K_4\ K_C/(K_2\ K_W)$	$mol^2\ m^{-6}$	Calculated
K_7	K_C/K_2	$mol^3\ m^{-9}$	Calculated
K_C	$10^{(13.870\ -\ 3059/T\ -\ 0.04035T)}$	$mol^2\ L^{-2}$	20
K_W	$\rho_W^2 10^{(-5839.50/T-22.4773\log T+61.2062)}$	$mol^2\ m^{-6}$	21
k_{11}	$10^{(13.635\ -\ 2895/T)}$	$L\ mol^{-1}\ s^{-1}$	22
k_{21}	6.0×10^6	$m^3\ mol^{-1}\ s^{-1}$	16
k_{31}	1.4×10^8	$m^3\ mol^{-1}\ s^{-1}$	16
k_{41}	$10^{(329.85\ -\ 110.541\log T\ -\ 17265.4/T)}$	s^{-1}	23
k_{51}	$10^{(0.198\ -\ 444/T)}$	$cm\ s^{-1}$	12
k_{61}	$10^{(2.84\ -\ 2177/T)}$	$cm\ s^{-1}$	12
k_{71}	$10^{(-5.86\ -\ 317/T)}$	$mol\ cm^{-2}\ s^{-1}$	12

TABLE 2 Base-case operating condition

Parameter	Value
Operating temperature and pressure	20°C, 1 atm
Diameter of reactor column	1 m
Gaseous CO_2 concentration at gas inlet, atmospheric	410 ppm
Concentrations at liquid inlet:	
$CO_{2(aq)}$	$1.646\times10^{-2}\ mol\ m^{-3}$
HCO_3^-	$2.556\times10^{-3}\ mol\ m^{-3}$
CO_3^{2-}	$4.180\times10^{-8}\ mol\ m^{-3}$
H^+	$2.559\times10^{-3}\ mol\ m^{-3}$
OH^-	$2.652\times10^{-6}\ mol\ m^{-3}$
Ca^{2+}	0

where a_{G-L} (m^{-1}) is the gas–liquid interfacial area per unit volume of the bed and K_{OL} (m/s) is the overall liquid phase mass-transfer coefficient. The saturated concentration of CO_2 in the liquid phase, $c^*_{CO_2(aq)}$ ($mol\ m^{-3}$), can be calculated by Henry's law:

$$c^*_{CO_2(aq)} = c_{CO_2(g)} RT/k_H \tag{25}$$

The expression used to determine the interfacial area for mass transfer depends on the pattern of interactions between the three phases. For a trickle flow bed, a commonly used expression based on Onda's work is[24,25]:

$$a_{G-L} = a_t\left\{1-\exp\left[-1.45\left(\frac{\sigma_C}{\sigma_L}\right)^{0.75}\mathrm{Re}_L^{0.1}Fr_L^{-0.05}We_L^{0.2}\right]\right\} \tag{26}$$

where σ_C ($N\ m^{-1}$) is the critical surface tension of the packing material ($2.17\times10^{-2}\ N\ m^{-1}$ at 20°C) and σ_L ($N\ m^{-1}$) is the surface tension of the liquid ($7.28\times10^{-2}\ N\ m^{-1}$ at 20°C).[26] Only a portion of the solid particles is wetted by the liquid flow in the trickle flow regime; the specific wetted area of the bed, a_w (m^{-1}), different from a_{G-L} and used in Equations (13), (16) and (17) for the weathering reactions, is given by[27]

$$a_w = a_t\left\{1-\exp\left[-1.986Fr_L^{0.139}Mo_L^{0.0195}\varepsilon_M^{-1.55}\right]\right\} \tag{27}$$

In the above equations, a_t (m^{-1}) is the total specific particle surface area of the packed bed, a function of particle diameter d_p (m) and bed porosity ε_M:

$$a_t = 6(1-\varepsilon_M)/d_p \tag{28}$$

For a random packing, bed porosity is calculated by[28]

$$\varepsilon_M = 0.390 + \frac{1.740}{(d_R/d_p+1.14)^2} \tag{29}$$

where d_R (m) is the diameter of the reactor.

For a trickle flow bed operated below the loading point, ε_L is given by[29,30]

$$\varepsilon_L = \left(12\frac{Fr_L}{\mathrm{Re}_L}\right)^{1/3} \tag{30}$$

The longitudinal dispersion coefficient is calculated from the following empirical correlation[31]:

$$\frac{1}{Pe_L} = \frac{Pe_m}{5}(1-p)^2 + \frac{Pe_m^2}{25}p(1-p)^3\left\{\exp\left[-\frac{5}{p(1-p)Pe_m}\right]-1\right\} + \frac{1}{\tau Pe_m} \tag{31}$$

with

$$p = \frac{0.48}{Sc^{0.15}} + \left(\frac{1}{2} - \frac{0.48}{Sc^{0.15}}\right)\exp\left(-\frac{75Sc}{Pe_m}\right) \tag{32}$$

where Pe_L and Pe_m are the Peclet number based on longitudinal dispersion coefficient and molecular diffusivity, respectively. Sc is the Schmidt number, and τ is the tortuosity of the packed bed.

$$Pe_L = \frac{\bar{u}_L d_p}{D_L}, Pe_m = \frac{\bar{u}_L d_p}{D_m}, Sc = \frac{\mu_L}{\rho_L D_m} \tag{33}$$

where $\bar{u}_L$ (m s^{-1}) is the mean interstitial liquid velocity, D_L and D_m (m^2 s^{-1}) are the longitudinal dispersion and molecular diffusion coefficients, respectively. The mean interstitial velocity is found from the liquid holdup, based on $\varepsilon_L = u_L/\bar{u}_L$. The tortuosity of a bed of randomly packed spherical particles can be estimated from[32]

$$\tau = 1.23\frac{(1-\varepsilon_M)^{4/3}}{\varepsilon_M} \tag{34}$$

K_{OL} (m s^{-1}) for the transfer of carbon dioxide is calculated from the following expression which takes the enhancement factor, E, into account[33]:

$$\frac{1}{K_{OL}} = \frac{1}{Ek_L} + \frac{RT}{k_H k_G} \tag{35}$$

where k_L and k_G (m s^{-1}) are the mass-transfer coefficients on the liquid and gas side, respectively. These are calculated from Onda's correlations[25]:

$$k_G = 5.23\left(\frac{\rho_G u_G}{a_t \mu_G}\right)^{0.7}\left(\frac{\mu_G}{\rho_G D_{G,m}}\right)^{1/3}(a_t d_p)^{-2.0} a_t D_G \tag{36}$$

$$k_L = 0.0051\left(\frac{\rho_L u_L}{a_{G-L}\mu_L}\right)^{2/3}\left(\frac{\mu_L}{\rho_L D_{L,m}}\right)^{-0.5}(a_t d_p)^{0.4}\left(\frac{\rho_L}{\mu_L g}\right)^{-1/3} \tag{37}$$

where $D_{G,m}$ and $D_{L,m}$ (m^2 s^{-1}) are the molecular diffusivity of CO_2 in gas and liquid, respectively. The dimensionless numbers used in this work include Re (Reynolds number), Fr (Froude number), We (Weber number), Mo (Morton number) and Ga (Galileo number). These are:

$$Re_L = \frac{u_L \rho_L}{a_t \mu_L}, Fr_L = \frac{u_L^2 a_t}{g}, We_L = \frac{u_L^2 \rho_L}{\sigma_L a_t}, Mo_L = \frac{g\mu_L^4}{\rho_L \sigma_L^3}, Ga_L = \frac{g\rho_L^2}{\mu_L^2 a_t^3} \tag{38}$$

where μ_L (Pa s) and ρ_L (kg m^{-3}) are the viscosity and density of liquid, respectively. g (m s^{-2}) is the acceleration due to gravity. Onda's correlations including Equations (26), (36) and (37) are valid for $0.04 < Re_L < 500$, $1.2 \times 10^{-7} < We_L < 0.27$ and $2.5 \times 10^{-9} < Fr_L < 1.8 \times 10^{-2}$.

2.5 | Enhancement factor

There are two chemical reactions, Equations (6) and (9), which, if occurring in the liquid film to any appreciable extent, will accelerate the rate of absorption of CO_2 above what would be expected from a purely physical absorption with the same concentration driving force. The factor by which the liquid film transfer coefficient is then increased is the enhancement factor, E, as shown in Equation (35). The calculation scheme for E used in this work is that developed by Hogendoorn et al[33] for reversible reactions of finite rate in chemically loaded solutions. It starts with estimation of the asymptotic or maximum attainable enhancement factor of a reversible (pseudo-)first-order reaction, E^∞, as given by

$$E^\infty = 1 + \frac{D_{HCO_3^-,L}\left(c_{HCO_3^-,I} - c_{HCO_3^-,L}\right)}{D_{CO_{2(aq)},L}\left(c_{CO_{2(aq)},I} - c_{CO_{2(aq)},L}\right)} \tag{39}$$

where D_i (m s^{-2}) and c_i (mol m^{-3}) are the molecular diffusivity and concentration of species i, the subscript I and L specifying gas–liquid interface and bulk liquid, respectively. To calculate E^∞ from Equation (39) requires the interfacial compositions of only four species, namely $CO_{2(aq)}$, HCO_3^-, H^+, and OH^-, since there is negligible conversion to carbonate. To find these, three equilibria are applied at the interface—Henry's law Equation (18), the CO_2 hydrolysis equilibrium Equation (9) and the ionic product of water Equation (8). The necessary fourth equation is provided by conservation of mass since the net generation rate of HCO_3^- is equal to the generation rate of H^+ plus the consumption rate of OH^-. Equating the rates of transfer between interface and bulk liquid we obtain:

$$D_{HCO_3^-,L}\left(c_{HCO_3^-,I} - c_{HCO_3^-,L}\right) = D_{H^+,L}\left(c_{H^+,I} - c_{H^+,L}\right) - D_{OH^-,L}\left(c_{OH^-,I} - c_{OH^-,L}\right) \tag{40}$$

Solving the three equilibria at the interface together with Equation (40), the particular interfacial concentrations $c_{CO_{2(aq)},I}$, $c_{HCO_3^-,I}$, $c_{H^+,I}$ and $c_{OH^-,I}$ can be found and E^∞ can then be calculated from Equation (39). As shown by Hoogendoorn et al,[33] this value of E^∞ enables us to use DeCoursey's expression originally derived for an *irreversible* reaction, for our cases of *reversible* reactions with a chemically loaded solution. The apparent enhancement factor for reaction n is calculated by DeCoursey's expression which is[34]:

$$E_n = -\frac{Ha_n^2}{2(E^\infty - 1)} + \sqrt{\left[\frac{Ha_n^4}{4(E^\infty - 1)^2} + \frac{E^\infty Ha_n^2}{(E^\infty - 1)} + 1\right]} \tag{41}$$

where Ha_n is the Hatta number for reaction n. For the reactions represented by Equations (6) and (9), the Hatta number is respectively expressed as[33,34]:

$$Ha_1 = \frac{\sqrt{k_{11} D_{CO_{2(aq)}} c_{OH^-,L}}}{k_L} \tag{42}$$

$$Ha_2 = \frac{\sqrt{k_{41} D_{CO_{2(aq)}}}}{k_L} \tag{43}$$

The overall enhancement factor of parallel reactions is calculated by the method of Gaspar and Fosbøl[35]:

$$E = 1 + \sum (E_n - 1) \tag{44}$$

2.6 | Determination of the applicable range of superficial velocities

Since the particles shrink during reaction and the liquid holdup increases as the particles get smaller, the EW process could potentially lead to flooding of the bed. Our chosen operating policy to counter this is to operate continuously at the same "distance" from the flooding limits (i.e., at a constant fraction of flood), which requires the operating gas and liquid velocities to be adjusted as a function of particle size. According to the correlations of Billet and Schultes,[29,30,36] the superficial gas velocity at the flooding point is given by:

$$u_{G,Fl} = \sqrt{2}\sqrt{\frac{g}{\psi_{Fl}}}\frac{(\varepsilon_M - \varepsilon_{L,Fl})^{3/2}}{\varepsilon_M^{1/2}}\sqrt{\frac{\varepsilon_{L,Fl}}{a_t}}\sqrt{\frac{\rho_L}{\rho_G}} \tag{45}$$

where ψ_{Fl} is the resistance coefficient and $\varepsilon_{L,Fl}$ is the liquid holdup, both at the flooding point. Note that $u_{G,Fl}$ is a function of the specific area in the bed, which is correlated with the size of the particles. ψ_{Fl} and $\varepsilon_{L,Fl}$ can be found from:

$$\psi_{Fl} = \frac{1}{C_{Fl}^2}\left[F_{lv}\left(\frac{\mu_L}{\mu_G}\right)^{0.2}\right]^{-2n_{Fl}} \tag{46}$$

where C_{Fl} and n_{Fl} are the constants for specific packing and F_{lv} is the flow parameter, a ratio defined by:

$$F_{lv} = \frac{u_L}{u_G}\sqrt{\frac{\rho_L}{\rho_G}} \tag{47}$$

When F_{lv} is smaller than 0.4, the liquid trickles downwards over the internals as a dispersed phase, while if F_{lv} is greater than 0.4, liquid in the void spaces tends to join up and flow down as a continuous phase.[30] In our work, the flow parameter is kept below 0.4. In this case, as suggested by Billet and Schultes,[30] $n_{Fl} = -0.194$. The value of the constant C_{Fl} was taken as 2.132, using the values for a wide range of column packings tabulated by Billet and Schultes[30] as a guide (60 values, mean $C_{Fl} = 2.006$, $SD = 0.291$).

The liquid holdup at the flooding point is determined by[29,30]:

$$\varepsilon_{L,Fl}^3(3\varepsilon_{L,Fl} - \varepsilon_M) = 6\varepsilon_M\frac{Re_{L,Fl}}{Ga_L} \tag{48}$$

Once the liquid holdup at the flooding point is known, the corresponding superficial liquid velocity at the flooding point, $u_{L,Fl}$, can be calculated using the following equation[29]:

$$u_{L,Fl} = \frac{g}{3}\frac{1}{a_t^2}\frac{\rho_L}{\mu_L}\varepsilon_{L,Fl}^3\left[1 - \frac{3}{2}\frac{(\varepsilon_M - \varepsilon_{L,Fl})}{\varepsilon_M}\right] \tag{49}$$

As pointed out by Billet and Schultes,[29] an iteration is needed to calculate $u_{G,Fl}$ and $u_{L,Fl}$ from these correlations. The iteration starts with F_{lv} (chosen for process reasons) as shown in Figure 2 Briefly, we first find $u_{L,Fl}$, using an initial guessed value $u^0_{L,Fl}$ which determines a corresponding value of $u_{G,Fl}$ according to Equation (47). We can then calculate $\varepsilon_{L,Fl}$ from Equation (48) and a new value for $u_{L,Fl}$from Equation (49). The procedure is repeated, replacing $u^0_{L,Fl}$ with the new value of $u_{L,Fl}$, until the match is sufficiently close, when $u_{L,Fl}$, $u_{G,Fl}$ and $\varepsilon_{L,Fl}$ will have been determined, for the given F_{lv}. The superficial liquid and gas velocities (u_L and u_G) applied in the reactor simulation should be a fraction of those at the flooding point. This fraction is termed the operating parameter, *OP*, in our work.

The superficial gas and liquid velocities at the flooding point of the trickle flow packed bed reactor at the selected F_{lv} and particle diameters, are shown in Figure 3. When operating at a constant flow parameter F_{lv}, as the particles become smaller both the gas and liquid velocities must be reduced proportionately to retain the same fraction of flood (i.e., same *OP*).

To save computational time, we have regressed the superficial velocity of liquid at the flooding point as a function of the flow parameter and particle size. The corresponding gas velocity is then also found:

$$u_{L,Fl} = a(d_p)^2 + b(d_p) + c \tag{50}$$

$$u_{G,Fl} = d \cdot u_{L,Fl} \tag{51}$$

The values of parameters *a*, *b*, *c*, *d* and the *R*-squared are shown in Table 3. The superficial velocities of gas and liquid at flooding point as a function of particle diameter can be found in Figure S1. Once the velocities at flooding are known for a particular flow parameter, it is straightforward to determine the velocities at a particular *OP*:

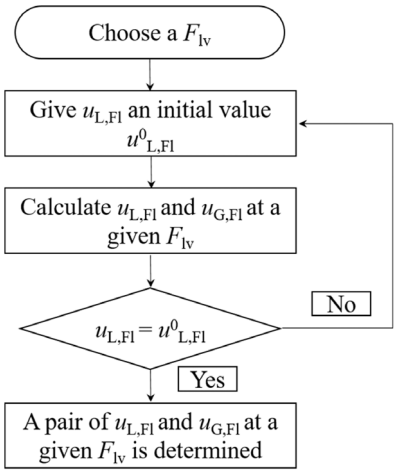

FIGURE 2 Iteration process to calculate superficial velocities of liquid and gas

$$u_L = OP \cdot u_{L,Fl}; u_G = OP \cdot u_{G,Fl} \quad (52)$$

2.7 | Calcite particle shrinkage by dissolution

The total mass loss rate (kg s^{-1}) of the solid is calculated by

$$\frac{dm}{dt} = M_p \cdot r_{Ca^{2+}} \cdot V_{bed} \quad (53)$$

where m (kg) is the total solid mass and V_{bed} (m^3) is the total volume of the packed bed. M_p (kg mol^{-1}) is the molecular weight of material dissolving out of the solid phase and $r_{Ca^{2+}}$ (mol m^{-3} s^{-1}) is the reaction rate computed by Equation (16) an average value for the bed since the particle shrinking rate is assumed to be location-independent. The density of the solids, ρ_s (kg m^{-3}), is 2,710 kg m^{-3} for calcite, so the rate of loss of solids volume may be found from Equation (53). The bulk density of the bed is ρ_s (1-ε_M) and the porosity is given by Equation (29), so the rate of change of bed volume and thus bed height at any point of the operation may also be found. The rate of change of particle diameter, r_{d_p} (m s^{-1}) and bed height, $r_{H_{bed}}$ (m s^{-1}) are then given by

$$r_{d_p} = \frac{1}{3}\frac{M_p r_{Ca^{2+}}}{\rho_s(1-\varepsilon_M)} d_p \quad (54)$$

$$r_{H_{bed}} = \frac{M_p r_{Ca^{2+}}}{\rho_s(1-\varepsilon_M)} \left(\frac{d_p}{d_p^0}\right)^3 H_{bed}^0 \quad (55)$$

where d_p^0 (m) and H_{bed}^0 (m) are the initial particle diameter and bed height, respectively.

Neglecting the insignificant change in porosity with particle diameter for large equipment, the particle diameter d_p is related to its initial value d_p^0 by.

$$d_p{}^3 = \left(d_p{}^0\right)^3 H_{bed}/H_{bed}^0 \quad (56)$$

To ensure that the same mass of calcite is dissolved from a given initial mass of solids when simulating batches with different initial particle sizes, the ratio of the terminal and initial particle diameter must be identical.

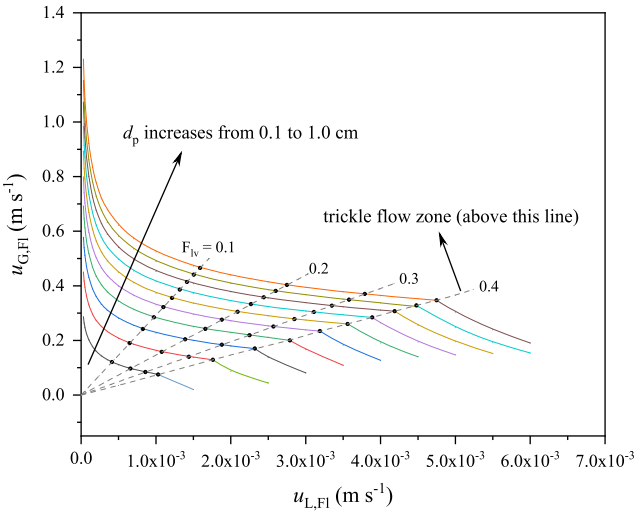

FIGURE 3 Superficial gas and liquid velocities at flooding with different particle diameters [Color figure can be viewed at wileyonlinelibrary.com]

2.8 | Energy and water consumption

We calculate energy and water consumption in this work considering only the operation of the reactor; other demands (e.g., the energy cost for rock grinding) are outside the scope of this assessment. More specifically, the energy required by the EW process as calculated here is for maintaining gas and liquid flow. Gas flowing through the bed must overcome the bed pressure drop which needs a blower or compressor. The energy input to this device, the work of compression, is

$$W_G = \frac{1}{\eta}\int_0^t \left\{ p_{in} Q_G^{in} \frac{\gamma}{\gamma - 1}\left[\left(\frac{p_{out}}{p_{in}}\right)^{\left(1-\frac{1}{\gamma}\right)} - 1\right]\right\} dt \quad (57)$$

where η is compressor efficiency, assumed to be 0.8. γ is the ratio of the specific heats at constant pressure and constant volume, Q_G^{in} (m^3 s^{-1}) is the inlet volumetric flow rate of gas, p_{in} (Pa) is the pressure of

TABLE 3 Parameters a, b, c, d and R^2 for regressed expression of gas and liquid velocities (m s^{-1}) at flooding in the packed bed

F_{lv}	a	b	c	d	R^2 Equation (50)	R^2 Equation (51)
0.10	−7.664	0.20965	2.4126×10^{-4}	292.996	.9999	1.0000
0.15	−11.702	0.30647	2.7032×10^{-4}	194.827	.9997	1.0000
0.20	−13.962	0.37630	3.4978×10^{-4}	146.501	.9978	1.0000
0.25	−17.418	0.46182	3.7826×10^{-4}	117.020	.9977	1.0000
0.30	−19.147	0.52315	4.2776×10^{-4}	97.603	.9979	1.0000
0.35	−22.129	0.59853	4.5637×10^{-4}	83.643	.9979	1.0000
0.40	−24.205	0.66346	4.7883×10^{-4}	73.254	.9981	1.0000

TABLE 4 Default values and range of studied parameters

Parameter (unit)	Default value	Range
Packed bed height (m)	10	1–60
Initial particle diameter (mm)	10	1.25, 2.5, 5, 10
Enhancement factor	Calculated by Equation (44)	1.0–5.0
$CO_{2(g)}$ concentration	410 ppm	410 ppm to 20%

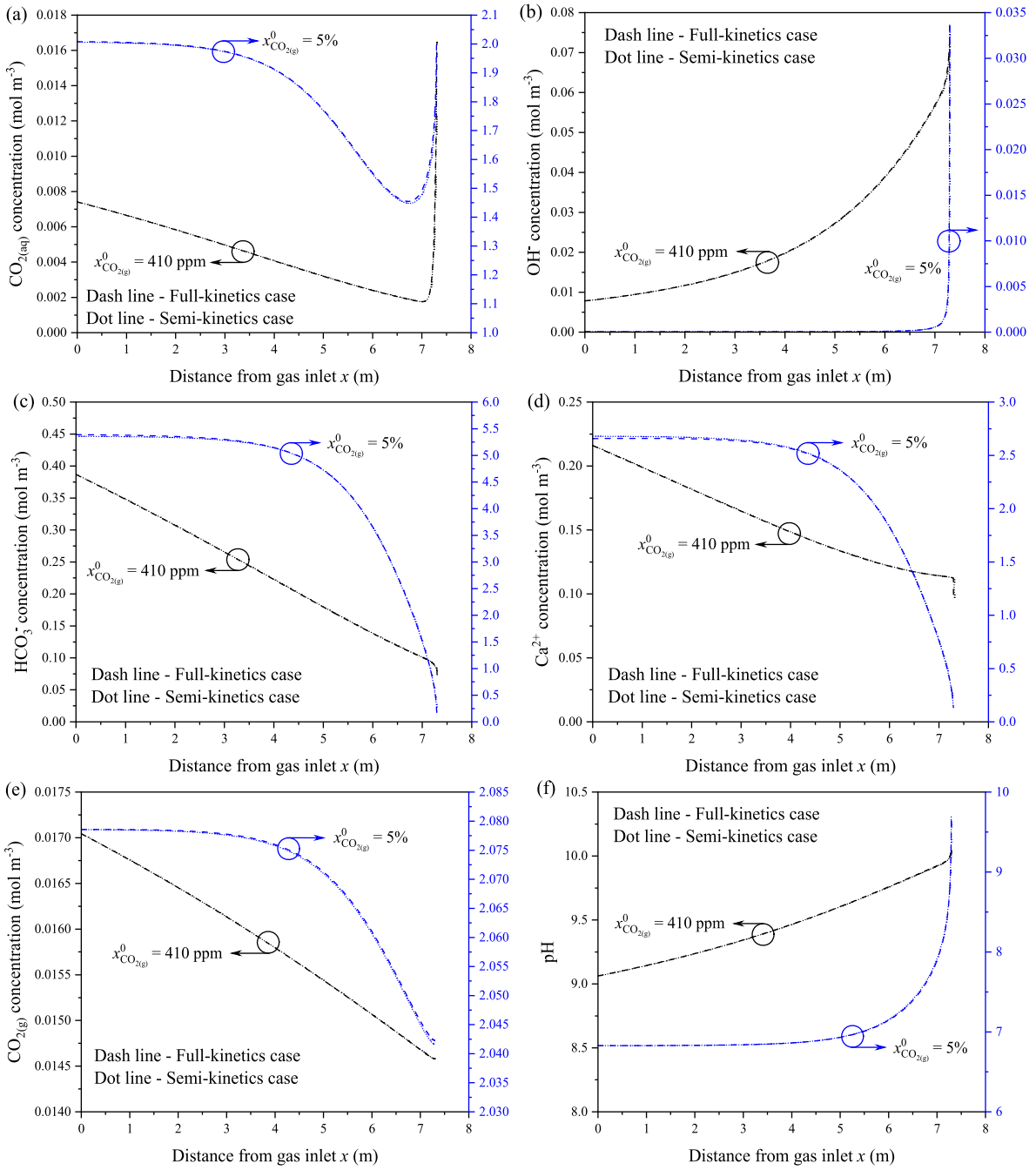

FIGURE 4 Composition within the packed bed with full-kinetics and semi-kinetics models in base-case operating condition. F_{lv} = 0.4, *OP* = 30%. Feed gas concentrations: 410 ppm and 5% CO_2. H_{bed} decreases from 10 to 7.3 m, d_p decreases from 10 to 9 mm. (a) $CO_{2(aq)}$, (b) OH^-, (c) HCO_3^-, (d) Ca^{2+}, (e) $CO_{2(g)}$, (f) pH [Color figure can be viewed at wileyonlinelibrary.com]

the feed stream to be compressed, generally close to atmospheric, p_{out} (Pa) is the pressure at the bottom of the bed, which is $p_{in} + \Delta p$.

The bed pressure drop is given by[30]

$$\frac{\Delta p}{H^{bed}} = \frac{\Delta p_0}{H^{bed}} \frac{\psi_L}{\psi_0} \frac{\varepsilon_M^3}{(\varepsilon_M - \varepsilon_L)^3} \tag{58}$$

where $\Delta p_0/H^{bed}$ (Pa m^{-1}) is the pressure drop per unit height of the dry bed. Details can be found in Billet and Schultes[30]; ψ_0 and ψ_L are the resistance coefficients of dry bed and wet bed respectively.

Water must be pumped to the top of the packed section, and the energy required, taking into account the decrease in bed height due to particle shrinkage, is

$$W_L = \frac{1}{\eta} \int_0^t \{\rho_L Q_L g H_{bed}\} dt \tag{59}$$

where Q_L (m^3 s^{-1}) is the volumetric flow rate of liquid, H_{bed} is the height of the bed. The efficiency η is again taken as 0.8.

The total energy consumption, summing that for gas compression and liquid pumping, is

$$W = W_G + W_L \tag{60}$$

The water consumption is calculated by the following equation:

$$V_L = \int_0^t u_L S_R dt \tag{61}$$

where S_R (m^2) is the cross-sectional area of the column.

2.9 | Meshing and numerical solution methods

Commercial software COMSOL Multiphysics 5.4 was employed to implement the fully coupled governing equations based on the finite element method (FEM) using a personal desktop with i7 processor and 32 GB RAM. In the COMSOL model, an adaptive mesh was mapped over the computational domain with finer resolution near the

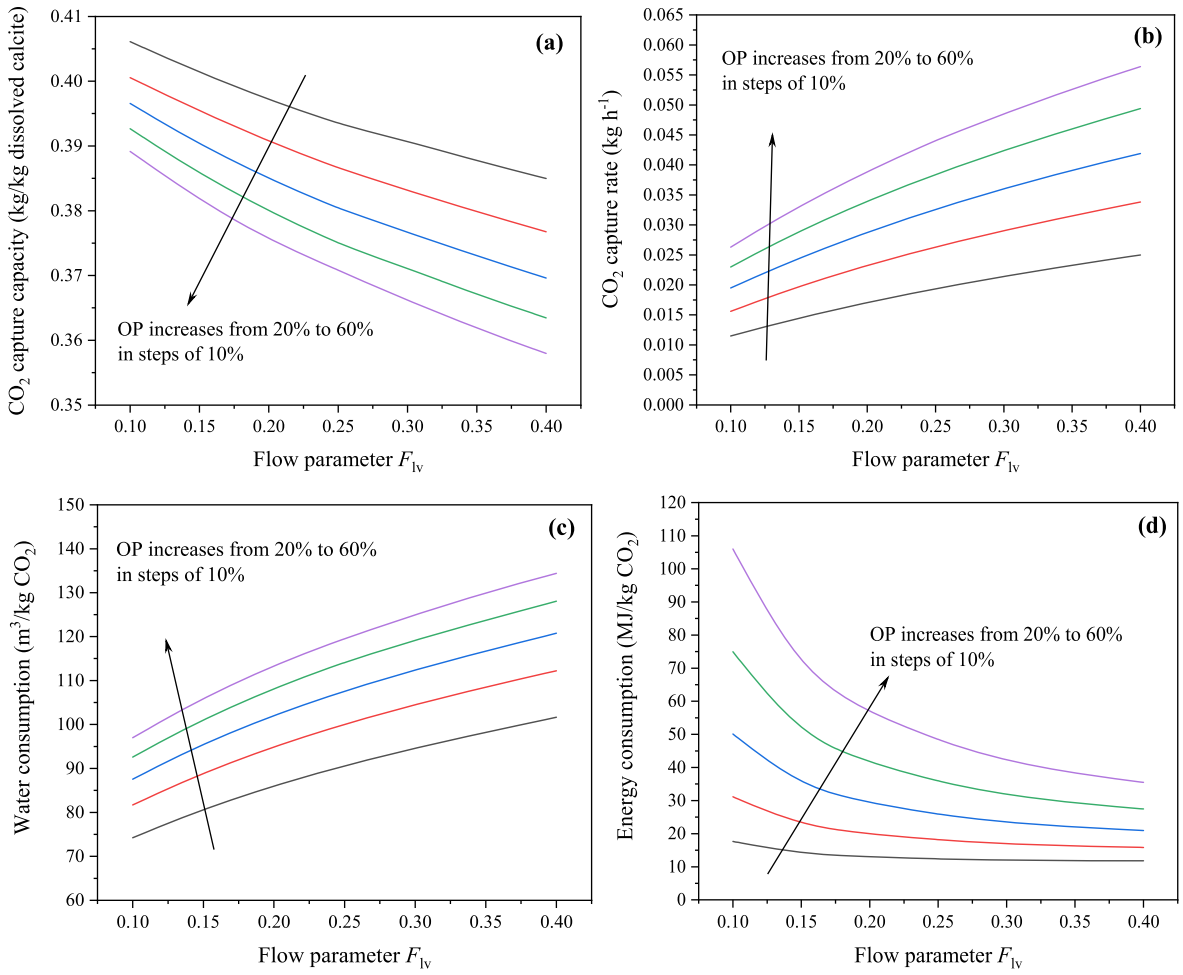

FIGURE 5 Effect of F_{lv} and OP on (a) CO_2 capture capacity, (b) CO_2 capture rate, (c) water consumption, and (d) Energy consumption. Base-case operating condition (Table 2) and the default values (Table 4) of other parameters apply [Color figure can be viewed at wileyonlinelibrary.com]

liquid inlet and coarser resolution toward the liquid outlet. The maximum element size is 0.1 m, the maximum element growth rate is 1.1, and the number of elements is 500 with an element ratio of 0.01 and a growth formula of arithmetic sequence. The MUMPS time-dependent solver of the software was adopted with default parameter settings, and the tolerance was set to be physics-controlled with a relative tolerance of 0.01.

3 | RESULTS AND DISCUSSION

The energy consumption, water consumption and CO_2 capture rate were studied as a function of flow parameter (F_{lv}), *OP*, initial packed bed height (H^0_{bed}) and initial particle diameter (d^0_p). Some calculations were also performed for a feed stream enriched with CO_2. To simulate the effect of a hypothetically accelerated liquid phase reaction, the enhancement factor (*E*) was also varied. Default values and range of varied input parameters are shown in Table 4. To avoid excessive computation time and without affecting the prediction of prominent trends, all reported simulations were carried out for partial (not full) dissolution of the particles, with the extent stated for each set of studies.

3.1 | Spatial distribution of species

Figure 4a–f show the variation of composition in the bed for two cases, one with air as the feed gas (bed exposure time 35,900 hr), and the other using air enriched with CO_2 to 5 mol% (bed exposure time 3,300 hr). Figure 4 shows the compositions when the particle diameter reached 90% of its initial value (d_p = 9 mm).

Water entering the bed is pre-saturated with CO_2 at atmospheric conditions (to give a concentration 0.01646 mol m^{-3}, see Table 2). Although the incoming water contains no calcium, at the top of the bed Ca^{2+} is present due to longitudinal dispersion in the liquid phase. Immediately below the liquid inlet, the chemical environment in the

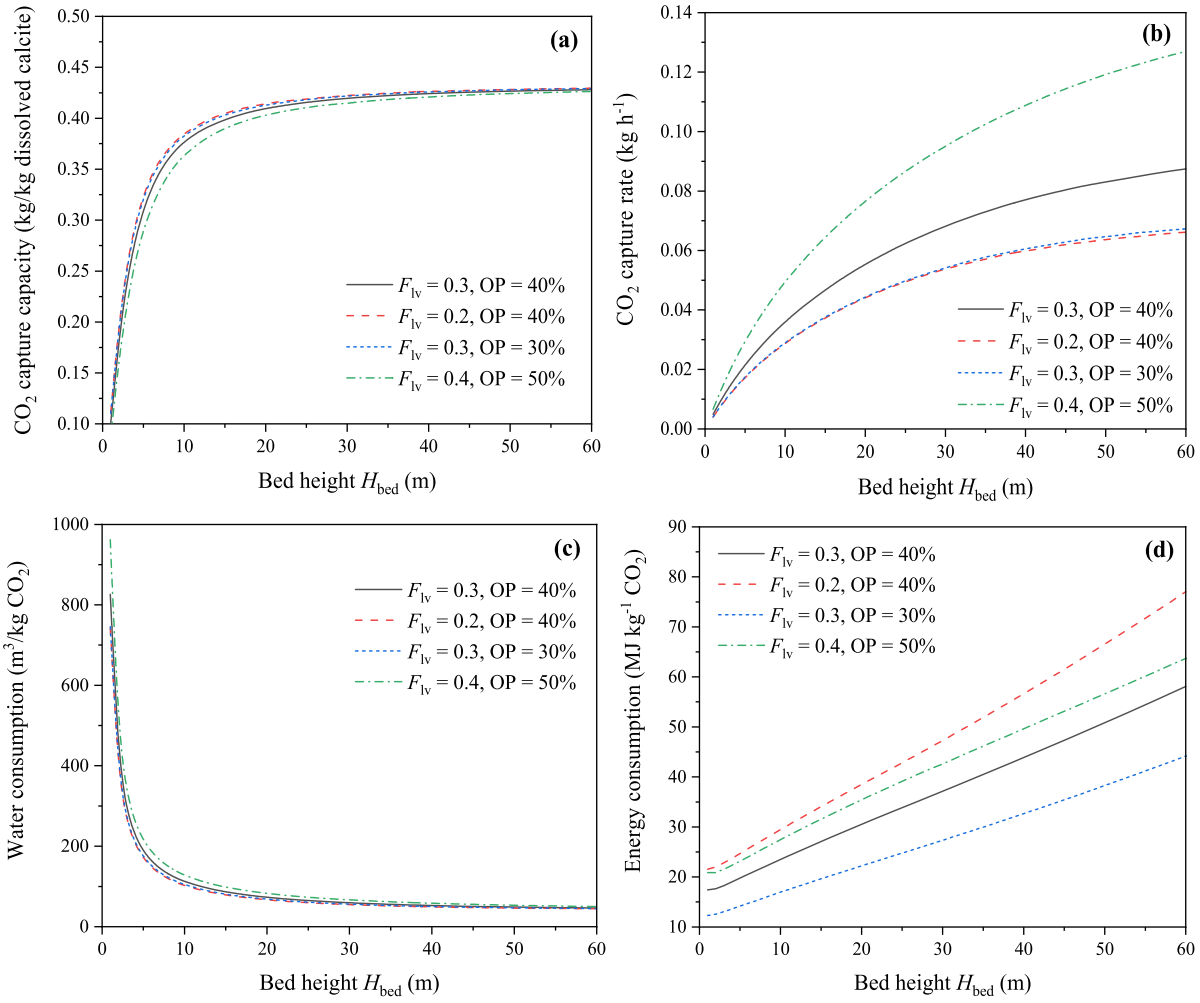

FIGURE 6 Effect of bed height on (a) CO_2 capture capacity, (b) CO_2 capture rate, (c) water consumption, and (d) Energy consumption. Base-case operating condition (Table 2) and the default values (Table 4) of other parameters apply [Color figure can be viewed at wileyonlinelibrary.com]

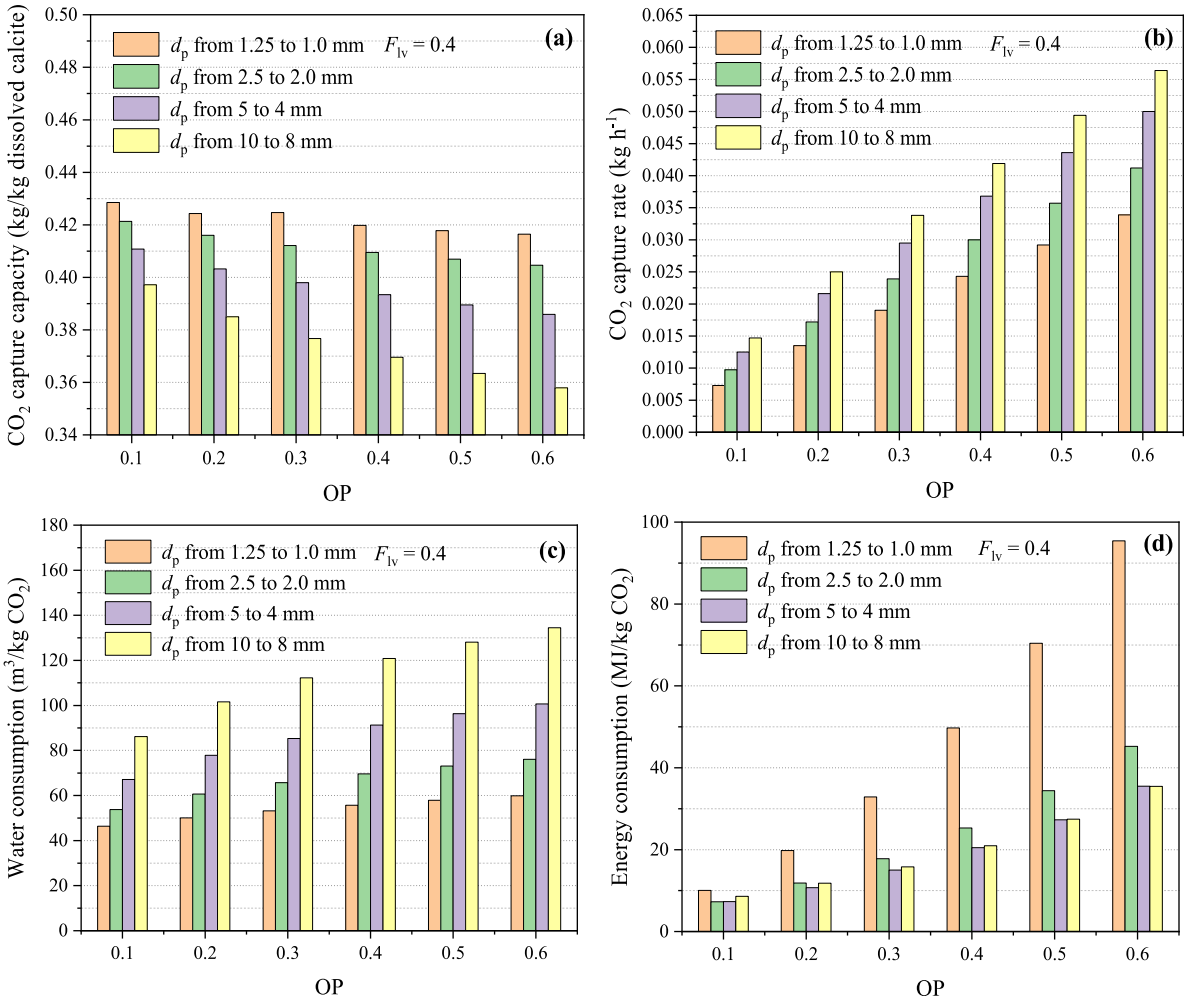

FIGURE 7 Effect of particle size on: (a) CO_2 capture capacity, (b) CO_2 capture rate (c) water consumption and (d) energy consumption. Base-case operating condition (Table 2) and the default values (Table 4) of other parameters apply [Color figure can be viewed at wileyonlinelibrary.com]

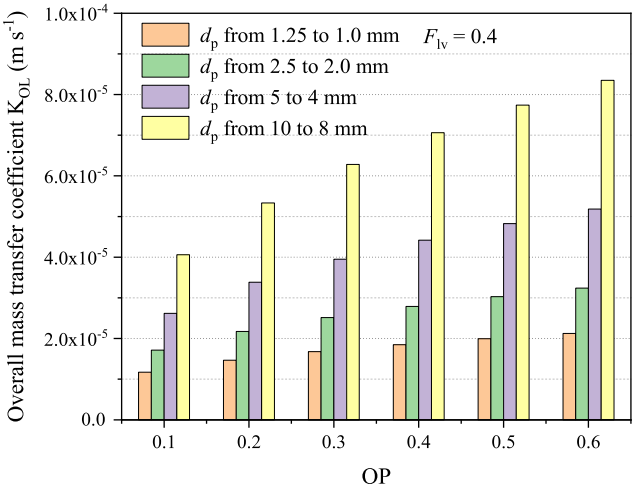

FIGURE 8 Effect of particle size on overall mass-transfer coefficient in base-case operating condition (Table 2) and the default value (Table 4) of other parameters [Color figure can be viewed at wileyonlinelibrary.com]

bed causes a sharp drop in the $CO_{2(aq)}$ and OH^- concentrations and a rise in bicarbonate concentration. Further down the bed, weathering of the solid particles causes concentrations of Ca^{2+} and bicarbonate to rise steadily in the trickling liquid, and $CO_{2(aq)}$ concentration also rises after its initial drop. The gas phase concentration of CO_2 decreases as this component is absorbed on rising through the bed, though the fractional removal is relatively modest here—18% for the air at 410 ppm CO_2, and 1.64% for the air enriched to 5% CO_2. In the latter case we can see that the lower half of the bed is rather inactive, there being a pinch at the bottom of the bed, where the liquid phase has become saturated with CO_2; evidently there is insufficient water flow to absorb much of the CO_2 being offered to the reactor. A greater value of the flow parameter is required, but F_{lv} = 0.4, the value used in Figure 4, is the maximum at which trickling flow can be maintained.

For the case shown in Figure 4 the change in CO_2 concentration is almost linear with height in both the liquid and gas phases over the lower 7 m of bed height. In this region the log mean concentration driving force for mass transfer can then be calculated, and from that

TABLE 5 Summary results of trickle flow bed for CO_2 capture through enhanced weathering (EW) in base-case operating condition

Parameter	Values for the least energy consumption (Case A)	Values for the least water consumption (Case B)	Values for the highest CO_2 capture rate (Case C)
Flow parameter F_{lv}	0.4	0.1	0.4
Operating parameter *OP*	10%	10%	60%
Particle diameter range (mm)	2.5–2.0	1.25–1.0	10.0–8.0
Total energy consumption (MJ/kg CO_2 captured)	7.26	33.15	35.47
Energy for water pumping W_L (% of total)	67.73	12.00	34.52
Energy for air blowing W_G (% of total)	32.27	88.00	65.48
Water consumption V_L (m^3/kg CO_2 captured)	53.75	43.11	134.5
Time required t (hr)	2.743×10^5	8.865×10^5	4.01×10^4
Average calcite dissolution rate (kg/m^2 surface area/hr)	2.36×10^{-6}	3.65×10^{-7}	6.45×10^{-5}
Average CO_2 capture rate (kg hr^{-1})	9.73×10^{-3}	3.07×10^{-3}	5.64×10^{-2}
Average mass-transfer coefficient K_{OL} (m s^{-1})	1.71×10^{-5}	8.36×10^{-6}	8.35×10^{-5}
Average superficial gas velocity u_G (m s^{-1})	1.25×10^{-2}	1.30×10^{-2}	0.186
Average superficial liquid velocity u_L (m s^{-1})	1.71×10^{-4}	4.43×10^{-5}	2.54×10^{-3}
Average packing specific area a_t (m^2 m^{-3})	1830.0	3660.0	457.4
Average gas–liquid interfacial area a_{G-L} (m^2 m^{-3})	70.67	65.33	78.54
Average interfacial area of the wetted area a_w (m^2 m^{-3})	1146.7	1923.3	375.49

Note: The average values are based on particle diameter from its initial size to the terminal size. Packed bed height: 10 m, initial atmospheric CO_2 concentration: 410 ppm. The ranges of studied parameters: (a) initial particle diameter: 1.25–10 mm; (b) flow parameter: 0.1–0.4; (c) operating parameter: 10–60%.

the height of a transfer unit (HTU). Commercial equipment for mass transfer in trickle flow generally provides an HTU of 1 m or less, though higher values may be expected when there is significant liquid phase resistance,[37] as in this case: Here the calculated value of HTU_{OG}, HTU based on the overall gas phase driving force, is 32 m. This is significantly poorer than most commercial absorbers because the absorbing component is not very soluble in the solvent, there is little chemical enhancement of transfer rate and the gas–liquid interfacial area is comparatively small.

In the "full-kinetics" case, all the participating chemical reactions (6)–(12) are dynamically modeled (see the additional rate expressions in the Supporting Information). In the "semi-kinetics" case the fast proton transfer reactions (7) and (8) are taken to be at equilibrium. Figure 4 shows that the calculated concentrations of various species with the semi-kinetics model are effectively identical to those with the full-kinetics model. Assuming equilibrium in reactions (7) and (8) reduces the complexity of the model and saves considerable computational time without significant loss of accuracy.

3.2 | Effect of flow parameter (F_{lv}) and *OP*

Figure 5a–d show four key performance indicators for trickle bed simulations in which the particle size was allowed to shrink from 10 to 8 mm, so that the bed decreased in height from 10 to 5.12 m. All the results are mean values averaged over the simulated period. A range of flow parameters and *OP* were chosen, to illustrate the effect of changes in velocities.

The total CO_2 capture capacity, defined as kg of CO_2 captured when 1 kg of calcite is dissolved, is shown in Figure 5a. According to the overall stoichiometry of the calcite reaction ($CaCO_3 + CO_2 + H_2O = Ca^{2+} + 2HCO_3^-$), 0.44 kg (or 10 mol) CO_2 would be captured for each kg (or every 10 mol) of calcite dissolved. We see that in all cases the capture capacity is close to this theoretical maximum. There is some loss in effectiveness of the use of dissolved calcite, more evident at higher flow parameters and higher *OP*. The calculated source terms of calcite dissolution, as shown in Figure S2, confirm that step (12) is the dominant process of calcite dissolution, generating the important OH^- ion that neutralizes H^+ and reacts with dissolved CO_2 in reaction step (6). Figure 4b shows that with atmospheric concentration of CO_2 in the feed gas, some OH^- ions can be washed out of the bed before they react. This will happen more at higher liquid flow rates, thus at larger F_{lv} and *OP*, and also with shorter beds.

The CO_2 capture rates are shown in Figure 5b. The results in Figure 4 suggest that the 8 m bed is not tall enough to make full use of the alkali generated by calcite dissolution. At the bottom of the bed the liquor is still some way from saturation with the incoming air (in Figure 4a, $x^0_{CO_2(g)} = 410$ ppm: $CO_{2(aq)} = 0.0074$ mol m^{-3} while saturation is 0.01646 mol m^{-3}). A faster CO_2 capture rate is achieved when larger F_{lv} and *OP* are used because parameters such as mass-transfer coefficients and interfacial areas increase. But as calcite particles

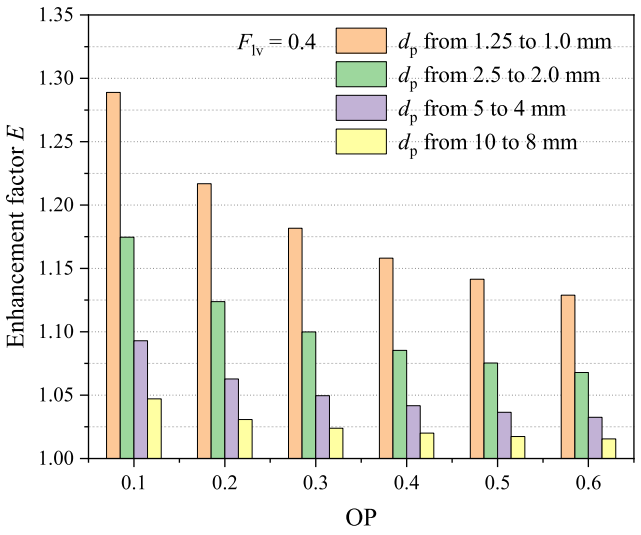

FIGURE 9 Effect of particle size on enhancement factor in base-case operating condition (Table 2) and the default value (Table 4) of other parameters [Color figure can be viewed at wileyonlinelibrary.com]

slowly shrink during the EW reaction, these parameters also decline as the liquid and gas velocities decrease (Figure S3). This leads to a reduced CO_2 capture rate as time passes.

The water consumption of the operation (volume of water used divided by mass of CO_2 captured) is shown in Figure 5c. The equilibrium concentration of Ca^{2+} in water at 20°C and 410 ppm CO_2 is 0.54 mol/m^3 so at saturation, 0.54 mol CO_2 would be captured by 1 m^3 of water according to the overall stoichiometry of the weathering reaction. Thus, the minimum water consumption is ~42.1 m^3 kg^{-1}. Figure 5c shows that the water consumption is always at least 50% greater than the minimum and becomes larger when F_{lv} and *OP* increase. The water consumption is least when the capture capacity is greatest, that is when F_{lv} and *OP* are least. Lower water consumption occurs with taller beds.

The energy consumption, (MJ of energy used divided by mass of CO_2 captured, is shown in Figure 5d. It comprises two parts as shown in Equation (60), of which the liquid pumping contribution is roughly proportional to the liquid flow rate (Equation 59). However, the gas compression part is roughly proportional to the gas flow rate squared (Equation 57) because the pressure drop in the packed bed increases with flow rate.[29] Both parts are proportional to the height of the bed, and to the duration of the batch. Figure 5d shows that energy consumption tends to increase as F_{lv} is reduced particularly at higher *OP*, where the energy needed for air compression becomes more dominant (Figure S4).

3.3 | Effect of bed height

The CO_2 capture capacity, Figure 6a, initially increases markedly as taller beds are used, but the rate of increase declines as the capture capacity approaches the theoretical maximum of 0.44 kg CO_2 per kg of calcite dissolved. The capacity is lower at larger F_{lv} and *OP*, but the effect of these parameters is relatively minor, as previously seen in Figure 5a (note the different y-axis scales between Figures 5a and 6a).

In our simulations which were each run at constant F_{lv} and constant *OP*, the liquid and gas superficial velocities are determined by particle size (Equations 50, 51 and 52). For various given initial bed heights, the initial and terminal particle sizes are fixed, so the volumetric flow rates of liquid and gas through beds of different height are the same. But the total amount of calcite dissolved out of a taller bed is greater, leading to a higher concentration of Ca^{2+} at liquid outlet, as shown in Figure S5. For example, as the bed height increases from 1.0 to 10 m, the Ca^{2+} concentration at the outlet increases from 0.118 to 0.215 mol/m^3. The increase in Ca^{2+} would lead to a larger CO_2 capture capacity at equilibrium because the final product of weathering is calcium bicarbonate. However, although plenty of calcite is dissolved in reaction step (12), the generated OH^- must be consumed by reaction step (6), which requires CO_2 to arrive by mass transfer from the gas phase. When the rate of mass transfer is insufficient, some of the generated Ca^{2+} and OH^- is flushed out of the bed without reacting with aqueous CO_2. This leads to the lower CO_2 capture capacity of shorter beds, which have less gas–liquid interfacial area for mass transfer.

The variation of CO_2 capture capacity with initial bed height is consistent with the increase in CO_2 capture rate shown in Figure 6b. As more bed height is added, more CO_2 capture occurs, and the effectiveness of extra bed height only decreases slowly, though of course there is an energy penalty, as shown in Figure 6d.

Figure 6c shows the effect of bed height on water consumption. With heights less than 7–8 m very large volumes of water are required, because the beds are short and there is too little CO_2 captured to utilize the dissolved calcite effectively. Figure 6c mirrors Figure 6a. As more bed height is added, the saturation level of the liquid increases, and the water consumption approaches the theoretical minimum, ~42.1 m^3/kg, when the effluent is at equilibrium with air at 410 ppm CO_2.

The energy consumption for both liquid pumping and gas blowing increase almost linearly with bed height, as shown in Figure 6d, which is a warning that the increase in CO_2 capture rate and reduced consumption of water in taller beds come at an energy cost. These results suggest that when the initial bed height is set at 7 m, the ratio of CO_2 capture capacity and energy consumption is at a maximum, which is perhaps an optimum. In this case, the water consumption is ~3 times the theoretical minimum and the CO_2 capture rate is around one third that calculated with a bed height of 60 m, but other trade-offs are also possible.

3.4 | Effect of particle size

When investigating the effect of particle size on the reactor performance, to obtain the same amount of calcite dissolution, the ratio of the particle diameters at the start and end of a run must be the same. We investigated four size ranges of the particle diameter, namely

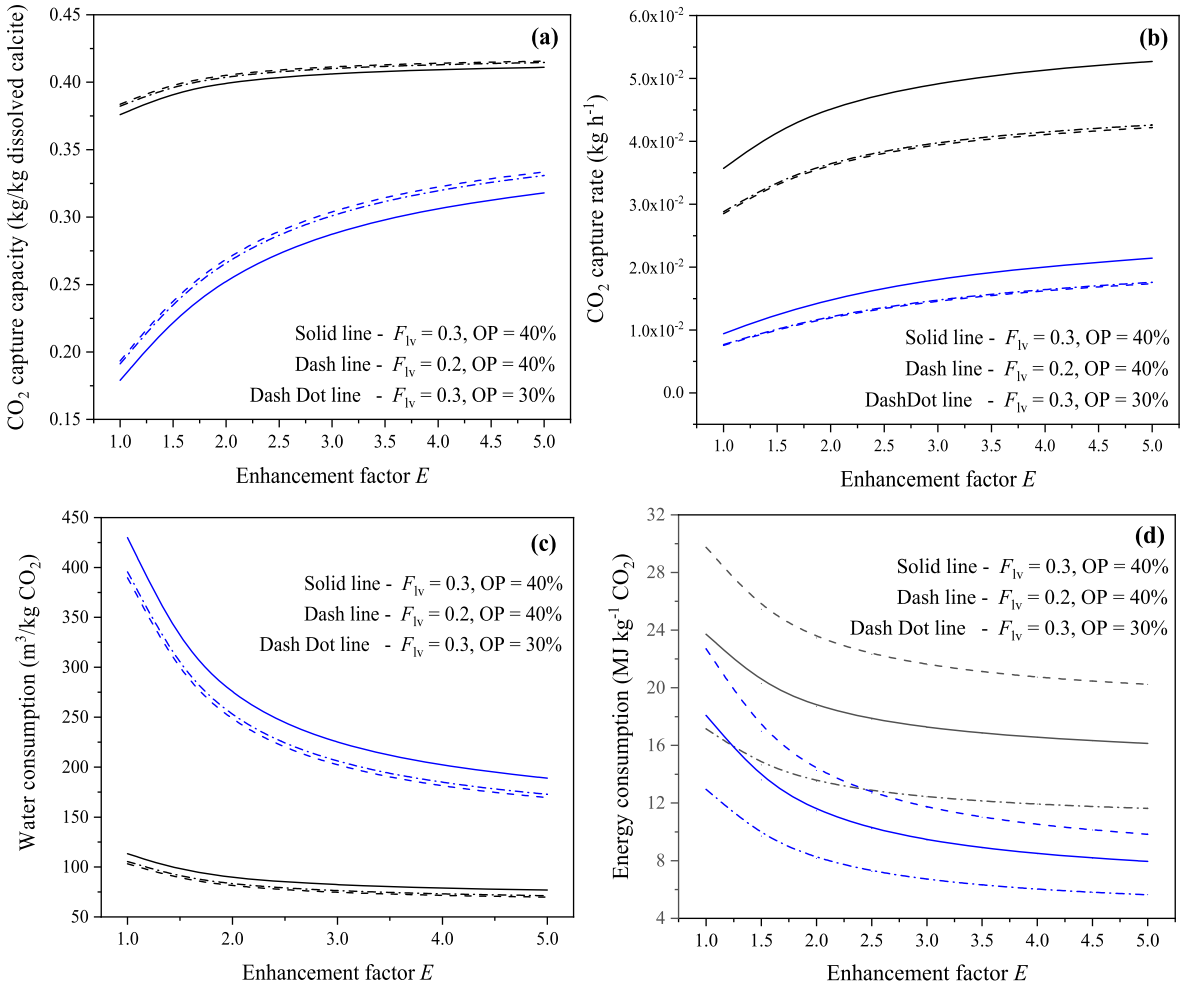

FIGURE 10 Effect of enhancement factor on energy consumption (a), CO_2 capture capacity (b), water consumption (c) and CO_2 capture rate (d) in base-case operating condition (Table 2). Black lines—H_{bed} = 10 m, blue lines—H_{bed} = 2 m, d_p^0 = 10 mm, $c^0_{CO_{2(g)}}$ = 410 ppm [Color figure can be viewed at wileyonlinelibrary.com]

dissolution from 10 to 8 mm, 5 to 4 mm, 2.5 to 2 mm and 1.25 to 1 mm at base-case operating condition with the default value of other parameters.

As shown in Figure 7a, the particle size has little effect on CO_2 capture capacity, though the capacity is somewhat higher with smaller particles due to the combination of potentially conflicting factors (e.g., increase in mass transfer area and decrease in the mass-transfer coefficient, cf. Figure 8). At these conditions the CO_2 capture capacity is close to the maximum value, 0.44 kg kg^{-1}. The increase in CO_2 capture rate seen in Figure 7b for the larger particle sizes occurs because the system operates in those cases at a higher velocity which increases mass-transfer coefficients, as shown in Figure 8. The absolute values of K_{OL} in Figure 8 are rather low compared with what would normally be expected in an industrial absorption process—in these packed beds of smallish spherical particles, there is little opportunity for the turbulence and convection that enhance transfer at the gas–liquid interface at higher gas velocities with high open-area packing. In fact, the values of K_{OL} here would be even lower but for the (modest) enhancement of mass transfer rates caused by reaction steps (6) and (9) which particularly help the beds of smaller particles—see Figure 8. The smaller particles, with their greater surface area, offer the advantage of lower water consumption for the same quantity of calcite dissolution, as shown in Figure 7c. However, with their lower operating velocities (and thus longer run times) and higher gas phase pressure drop (see Figure S6), the smaller particles can have a significant energy penalty, as demonstrated in Figure 7d.

3.5 | Results of optimizing strategies

Table 5 summarizes simulation results where the flow parameter F_{lv}, operating parameter *OP* and particle size were varied according to three different optimizing strategies, seeking (a) least energy consumption, (b) least water consumption, and (c) highest CO_2 capture rate. The least energy consumption, 7.26 MJ/kg CO_2, is found at an intermediate particle size with the largest F_{lv} and smallest *OP*, and a water consumption only slightly (25%) more than the minimum value. The other two optima incur an energy consumption 4–5 times greater. The highest CO_2 capture rate gives much the lowest batch time, with the largest particles. This limited search for optimal operating

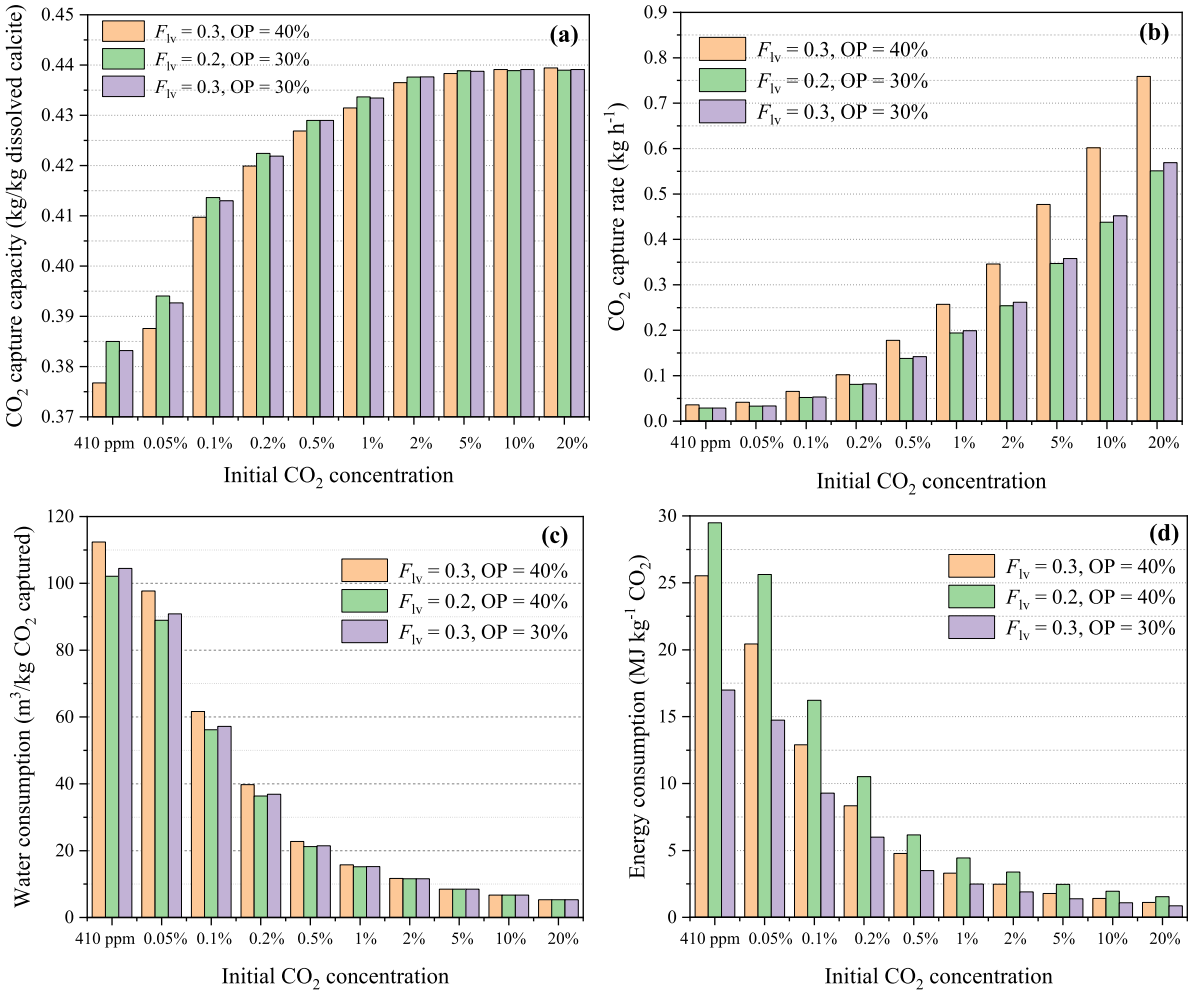

FIGURE 11 Effect of feed CO_2 concentration on: (a) CO_2 capture capacity, (b) CO_2 capture rate, (c) water consumption and (d) energy consumption in base-case operating condition (Table 2) and the default value (Table 4) of other parameters [Color figure can be viewed at wileyonlinelibrary.com]

conditions illustrates the kind of trade-offs that can be made, and Table 5 shows typical values for some of the key variables in a trickle flow reactor. A wider search for optimal operations should include other types of reactor such as slurry columns, but this is outside the scope of the present work.

The height of an overall gas phase mass transfer unit (HTU_{OG}) can be calculated for the average values given in Table 5, with $HTU_{OG} = u_G k_H/(K_{OL} \cdot RT \cdot a_{G-L})$. The values for cases A, B and C are 11, 25 and 29 m respectively. These rather large values again reflect the poor solubility of CO_2 (large k_H), and the low gas–liquid interfacial area.

The simulations of these three optimizing strategies can also be used to analyze the relative importance of mass transfer and chemical reactions as the rate-controlling mechanisms. Among the chemical reactions, Equations (6), (9) and (11) are the routes by which dissolved CO_2 (that is, $CO_{2(aq)}$) is removed from the liquid phase. At the pH of the solutions in this weathering system (with CO_2 supplied at 410 ppm), Equation (6) makes negligible contribution to the removal of $CO_{2(aq)}$. Considering only forward reactions for the sake of a simplified analysis, the rate of chemical reaction of dissolved CO_2 in unit volume of bed is thus approximately given by

$$r_{CO_2(aq)} = k_{41} c_{CO_2(aq)} \varepsilon_L + k_{61} c_{CO_2(aq)} a_w \tag{62}$$

The maximum rate of chemical reaction is then

$$r_{CO_2(aq)} = k_{41} c^*_{CO_2(aq)} \varepsilon_L + k_{61} c^*_{CO_2(aq)} a_w \tag{63}$$

And the maximum rate of mass transfer, from Equation (24) is

$$r_{G-L} = a_{G-L} K_{OL} c^*_{CO_2(aq)} \tag{64}$$

We can expect the rate of EW to be limited by the gas–liquid mass transfer when $r_{G-L} \ll r_{CO_2(aq)}$. That is, the mass transfer is limiting when

$$\frac{a_{G-L} K_{OL}}{k_{41} \varepsilon_L + k_{61} a_w} << 1 \tag{65}$$

Calculated from the data in Table 5, the values of the left-hand-side expression for Cases A, B and C are 0.041, 0.011 and 0.59, respectively. These values imply that the rate of EW in Cases A and

B is primarily controlled by the rate of gas–liquid mass transfer. In Case C, both the weathering reactions and the mass transfer have similar rates, so both play a role. The criterion (65) demonstrates the importance of chemical rates, but also mass-transfer coefficients and the characterizing parameters a_{G-L}, ε_L and a_w. Cases like A and B would obviously benefit more from enhancement of gas to liquid mass transfer, than cases like C. The approach of this analysis is general and could be applied to other weathering systems with known kinetics.

3.6 | Accelerating mass transfer by chemical reaction

For an absorption process like the one discussed here in which liquid phase mass transfer is a limiting factor, the acceleration of rates offered by chemical reaction in the liquid may prove crucial to viability. Reactions naturally occurring in the aqueous calcite system offer only a small enhancement (Figure 9) whereas many commercial absorptions make use of catalysis or additives which have a much larger effect. This may be difficult to accomplish in practice in EW, but we have examined theoretically the potential benefits in our model. We disabled the routines which calculated the enhancement factor (Section 2.5) and chose instead values of E in the range of 1.0–5.0. As shown in Figure 10a,b, an increase in enhancement factor improves the capture capacity and capture rate as if the bed had been made taller. However, this has occurred without any increase in the bed height, so there is a reduction in energy consumption, which is more pronounced for the shorter bed (Figure 10d). There is also a useful reduction in water consumption (Figure 10c). It is observable that the rate of improvement declines as E increases, and for enhancement factors greater than 3.0, there is little further benefit to energy or water consumption especially with the smaller bed height. Further simulation analysis (results not shown here) has confirmed that under these conditions the role of calcite dissolution in rate controlling becomes more significant.

3.7 | Weathering with CO_2-enriched air

The effect of initial CO_2 concentration, in the range of 410 ppm to 20%, on the reactor performance is shown in Figure 11 a–d. The CO_2 capture capacity and capture rate are both greater at higher feed CO_2 concentration as the rate of mass transfer of CO_2 from gas into liquid is enhanced by a higher CO_2 partial pressure. We see that increasing the feed gas CO_2 concentration from 410 ppm to even 0.5% reduces the energy and water consumption by 80%, and raising it again to 5% causes a further halving (Figure 11c,d). These results confirm the suggestion of Keleman et al[38] that reaction times would be significantly reduced when utilizing air enriched to a few percent in carbon dioxide to sparge through reacting alkaline rock.

4 | CONCLUSIONS

We conclude that a computerized advection-reaction-dispersion model can be developed for the EW of calcite with CO_2 and water in a trickle bed reactor with air through-flow. Performance indicators including CO_2 capture capacity and rate as well as water and energy requirements could be calculated from the model, and are shown to be influenced by factors such as bed height, particle size and the velocities of gas and liquid flows. In particular, the model shows that a bed height of at least 7–8 m is needed to enable sufficient weathering and thus capture of CO_2 with 1–10 mm particles. The simulation is possible because the dissolution and reaction kinetics of this mineralogical system have been well researched by many previous workers, and data fitted with theory and correlations as needed in the modeling. Given the importance of EW as a CDR technology, similar investigation of other minerals—dissolution and reaction kinetics—is urgently recommended. The model also requires mass transfer and hydrodynamic parameters for packed beds of particles, and again we have been able to use well-known results of previous workers, though extrapolation is needed to estimate properties of beds of rock particles. The hydrodynamic and mass transfer behavior of such mineral beds also deserves much more attention, if, as has been suggested, we are to apply EW at the scale required to capture gigatons per year of carbon dioxide. An important feature of the model is its ability to calculate the chemical enhancement of mass transfer through application of the results of Hogendoorn et al,[33] DeCoursey[34] and Gaspar and Fosbøl.[35] The relatively simple estimation method described here means that the computer model can be used to screen the performance of EW reactors with a reduced need for experimentation—though of course verification of this is needed. The computer model is able to deal with shrinkage of the bed which results from dissolution of the solids, and this is another topic that would benefit from further experimental research. The model shows that even a small enrichment of the CO_2 concentration of the inlet air, perhaps to as little as 0.5%, would make a significant saving in energy and water requirements of EW. Research to develop such schemes might be fruitful.

ACKNOWLEDGMENTS

The authors acknowledge the financial support by the Greenhouse Gas Removal by Enhanced Weathering (GGREW) project (grant No. NE/P01982X/1) funded by the Natural Environment Research Council (NERC) of the United Kingdom.

AUTHOR CONTRIBUTIONS

Lei Xing: Conceptualization; data curation; formal analysis; investigation; methodology; writing-original draft. **Richard Darton:** Formal analysis; methodology; project administration; supervision; writing-review and editing. **Aidong Yang:** Conceptualization; formal analysis; funding acquisition; methodology; project administration; supervision; writing-review and editing.

NOTATION

S	area, m^2
$\bar{u}$	average interstitial velocity, m s^{-1}
c	concentration, mol m^{-3}

d diameter, m
D diffusion coefficient, $m^2\ s^{-1}$
E enhancement factor
K equilibrium constant
F_{lv} flow parameter
Fr Froude number
Ga Galileo number
Ha Hatta number
H height, m
HTU height of transfer unit
k_H Henry's constant, pa $m^3\ mol^{-1}$
h holdup
m mass, kg
M molecular weight, kg mol^{-1}
Mo Morton number
n number
OP operating parameter, fraction of flood
C_p packing constant
Pe Peclet number
p pressure, Pa
k rate constant/mass-transfer coefficient
r reaction source/sink, mol $m^{-3}\ s^{-1}$
Re Reynolds number
Sc Schmidt number
a specific/interfacial area, m^{-1}
u superficial velocity, m s^{-1}
T temperature, K
t time, s
V volume, m^3
Q volumetric flow rate, $m^3\ s^{-1}$
We Weber number
W work/energy, J

Subscript

0 dry bed
aq aqueous
Fl flooding
G gas
I interface
i species i
L liquid
M mean
m molecular
OG overall gas phase driving force
p particle
R reactor
s solid phase
t total
w wetted

Greek

ρ density, kg m^{-3}
η efficiency
ε porosity
γ ratio of the specific heat
ψ resistance coefficient
σ surface tension, N/m
τ tortuosity
μ viscosity, Pa s

Superscript

* saturated
0 initial
∞ maximum

ORCID

Lei Xing https://orcid.org/0000-0002-0360-8025

REFERENCES

1. Dlugokencky EJ, Hall BD, Montzka SA, Dutton G, Mühle J, Elkins JW. Atmospheric composition [in *State of the Climate in 2018*, Chapter 2: Global Climate]. *Bull Amer Meteor Soc*. 2019;100:S48-S50.
2. Matthews HD, Zickfeld K, Knutti R, Allen MR. Focus on cumulative emissions, global carbon budgets and the implications for climate mitigation targets. *Environ Res Lett*. 2018;13:010201.
3. IPCC. Summary for policymakers. In: Masson-Delmotte V, Zhai P, Pörtner HO, et al., eds. *Global Warming of 1.5°C. An IPCC Special Report on the Impacts of Global Warming of 1.5°C Above Pre-Industrial Levels and Related Global Greenhouse Gas Emission Pathways, in the Context of Strengthening the Global Response to the Threat of Climate Change, Sustainable Development, and Efforts to Eradicate Poverty*. Geneva, Switzerland: World Meteorological Organization; 2018:32.
4. Minx JC, Lamb WF, Callaghan MW, et al. Negative emissions—part 1: research landscape and synthesis. *Environ Res Lett*. 2018;13:063001.
5. Schuiling RD, Krijgsman P. Enhanced weathering: an effective and cheap tool to sequester CO_2. *Clim Change*. 2006;74:349-354.
6. Strefler J, Amann T, Bauer N, Kriegler E, Hartmann J. Potential and costs of carbon dioxide removal by enhanced weathering of rocks. *Environ Res Lett*. 2018;13:034010.
7. Renforth P, Manning DAC, Lopez-Capel E. Carbonate precipitation in artificial soils as a sink for atmospheric carbon dioxide. *Appl Geochem*. 2009;24:1757-1764.
8. Renforth P, Pogge von Strandmann PAE, Henderson GM. The dissolution of olivine added to soil: implications for enhanced weathering. *Appl Geochem*. 2015;61:109-118.
9. Beerling DJ, Kantzas EP, Lomas MR, et al. Potential for large-scale CO2 removal via enhanced rock weathering with croplands. *Nature*. 2020;583:242-248.
10. Montserrat F, Renforth P, Hartmann J, Leermakers M, Knops P, Meysman FJR. Olivine dissolution in seawater: implications for CO_2 sequestration through enhanced weathering in coastal environments. *Environ Sci Technol*. 2017;51:3960-3972.
11. Hamilton JL, Wilson SA, Morgan B, et al. Accelerating mineral carbonation in ultramafic mine tailings via direct CO_2 reaction and heap leaching with potential for base metal enrichment and recovery. *Econ Geol*. 2020;115:303-323.
12. Plummer LN, Wigley TML, Parkhurst DL. The kinetics of calcite dissolution in CO_2-water system at 5 ° to 60 °C and 0.0 to 1.0 atm CO_2. *Amer J Sci*. 1978;278:179-216.
13. Buhmann D, Dreybrodt W. The kinetics of calcite dissolution and precipitation in geologically relevant situations of karst areas 1. Open system. *Chem Geol*. 1985;48:189-211.
14. Dreybrodt W, Lauckner J, Liu Z, Svensson U, Buhmann D. The kinetics of the reaction $CO_2 + H_2O \rightarrow H^+ + HCO_3^-$ as one of the rate

limiting steps for the dissolution of calcite in the system H_2O- CO_2-$CaCO_3$. *Geochim Cosmochim AC*. 1996;60:3375-3381.
15. Danckwerts PV. Continuous flow systems: distribution of residence times. *Chem Eng Sci*. 1953;2:1-13.
16. Gents AHG, Brilman DWF, Versteeg GF. CO_2 absorption in carbonate/bicarbonate solutions: the Danckwerts-criterion revisited. *Chem Eng Sci*. 2005;60:5830-5835.
17. Plummer L, Busenberg E. The solubilities of calcite, aragonite and vaterite in the CO_2-H_2O solutions between 0 and 90 °C, and an evaluation of the aqueous model for the system $CaCO_3$-CO_2-H_2O. *Geochim Cosmochim AC*. 1982;46:1011-1040.
18. Hikita H, Asai S, Takatsuka T. Absorption of carbon dioxide into aqueous sodium hydroxide and sodium carbonate-bicarbonate solutions. *Chem Eng J*. 1976;11:131-141.
19. Edwards TJ, Maurer G, Newman J, Prausnitz JW. Vapor-liquid equilibria in multicomponent aqueous solutions of volatile weak electrolytes. *AIChE J*. 1978;24:966-976.
20. Jacobson RL, Langmuir D. Dissociation constants of calcite and $CaHCO_3^+$ from 0 to 50 °C. *Geochim Cosmochim AC*. 1974;38:301-318.
21. Tsonopoulos C, Coulson DM, Inman LB. Ionization constants of water pollutants. *J Chem Eng Data*. 1976;21:190-193.
22. Pinsent BRW, Pearson L, Roughton FJW. The kinetics of combination of carbon dioxide with hydroxide ions. *T Faraday Soc*. 1956;52:1512-1520.
23. Danckwerts PV, Sharma MM. The absorption of carbon dioxide into solutions of alkalis and amines (with some notes on hydrogen sulphide and carbonyl sulphide). *Chem Eng*. 1966;CE244-CE280.
24. Onda K, Takeuchi H, Okumoto Y. Mass transfer coefficients between gas and liquid phases in packed columns. *J Chem Eng Jpn*. 1968;1:56-62.
25. Dvorak BI, Lawler DF, Fair JR, Handler NE. Evaluation of the Onda correlations for mass transfer with large random packings. *Environ Sci Technol*. 1996;30:945-953.
26. Shafrin EG, Zisman WA. Critical surface tension for spreading on a liquid substrate. *J Phys Chem*. 1967;71:1309-1316.
27. Julcour-Lebigue C, Augier F, Maffre H, Wilhelm AM, Delmas H. Measurements and modelling of wetting efficiency in trickle-bed reactors: liquid viscosity and bed packing effects. *Ind Eng Chem Res*. 2009;48(14):6811-6819.
28. Benyahia F, O'Neill KE. Enhanced voidage correlations for packed beds of various particle shapes and sizes. *Particul Sci Technol*. 2005;23:169-177.
29. Billet R, Schultes M. Fluid dynamics and mass transfer in the total capacity range of packed columns up to the flood point. *Chem Eng Technol*. 1995;18:371-379.
30. Billet R, Schultes M. Prediction of mass transfer columns with dumped and arranged packings—updated summary of the calculation method of Billet and Schultes. *Trans IChemE*. 1999;77:498-504.
31. Delgado JMPQ. A critical review of dispersion in packed beds. *Heat Mass Trans*. 2006;42:279-310.
32. Lanfrey PY, Kuzeljevic ZV, Dudukovic MP. Tortuosity model for fixed beds randomly packed with identical particles. *Chem Eng Sci*. 2010;65:1891-1896.
33. Hogendoorn JA, Bhat RDV, Kuipers V, vas Swaaij WPM, Versteeg GF. Approximation for the enhancement factor applicable to reversible reactions of finite rate in chemically loaded solutions. *Chem Eng Sci*. 1997;52:4547-4559.
34. DeCoursey WJ. Absorption with chemical reaction: development of a new relation for the Danckwerts model. *Chem Eng Sci*. 1974;29:1867-1872.
35. Gaspar J, Fosbøl PL. Practical enhancement factor model based on GM for multiple parallel reactions: piperazine (PZ) CO_2 capture. *Chem Eng Sci*. 2017;158:257-266.
36. Piche S, Larachi F, Grandjean BPA. Improved liquid hold-up correlation for randomly packed towers. *Trans IChemE*. 2001;79:71-80.
37. Treybal RE. *Mass-Transfer Operations*. New York: McGraw-Hill; 1980.
38. Kelemen PB, McQueen N, Wilcox J, Renforth P, Dipple G, Vankeuren AP. Engineered carbon mineralization in ultramafic rocks for CO_2 removal from air: review and new insights. *Chem Geol*. 2020;550:119628.

SUPPORTING INFORMATION

Additional supporting information may be found online in the Supporting Information section at the end of this article.

How to cite this article: Xing L, Darton RC, Yang A. Enhanced weathering to capture atmospheric carbon dioxide: Modeling of a trickle-bed reactor. *AIChE J*. 2021;67:e17202. https://doi.org/10.1002/aic.17202